Coulomb-Friction-Based Needle Insertion/Withdrawal Model And Its Discrete-Time Implementation

Conference Paper · July 2006

CITATIONS
3

READS
63

3 authors, including:

Ryo Kikuuwe
Hiroshima University
122 PUBLICATIONS **847** CITATIONS

SEE PROFILE

Coulomb-Friction-Based Needle Insertion/Withdrawal Model And Its Discrete-Time Implementation

Ryo Kikuuwe* Yu Kobayashi Hideo Fujimoto

Nagoya Institute of Technology, Nagoya, Aichi 466-8555, Japan

Abstract

This paper presents an analytical model of resistance force experienced through a needle when it is being inserted into and withdrawn from membranes. Though the model is based on a very simple assumption of linear elasticity and Coulomb friction, it well captures the 'pop' feature, which is a sudden loss of resistance force felt when the needle tip penetrates a membrane. This model describes the needle resistance force as a Coulomb-like friction that involves static friction and kinetic friction. For implementation in haptic devices, a discrete-time representation of this model is derived by using the implicit Euler scheme. The results of implementation experiments using a PHANTOM Omni device are presented.

1 Introduction

Needle insertion is one of the most important and basic tasks for medical operations. Many attempts have been made to utilize haptic virtual reality technology for the training of needle insertion procedures, such as intravenous injection [1] and epidural injection [2]. During a needle insertion, it is well known that a sudden change is felt in the resistance force when the needle punctures a membrane or a tissue. This change in the resistance force is usually referred to as a 'pop.' In the case of intravenous injection, for example, the operator can feel a pop when the needle enters the vein. The feeling of a pop can be considered as a reliable sign that the needle successfully reaches a target.

Many attempts are made to model a pop for the purpose of simulations involving haptic feedback. Brett et al. [3] measured needle forces during epidural insertion on porcine samples, and constructed a model by using an incremental viscoelastic model and empirical look-up tables. Kataoka et al. [4] measured the force acting on the needle tip from the force acting on the side wall of the needle independently. Okamura et al. [5] modeled the force as the sum of friction force, elastic force, and cutting force. In these researches, implementation in haptic interfaces is not considered. A CathSim AccuTouch device of Immersion Medical is known to be capable of producing haptic feedback including a pop. This device incorporates a magnetic brake to generate a one-DOF passive force feedback [6].

One major factor of needle resistance force is Coulomb friction force between the needle and the membrane to be punctured. Because Coulomb friction is discontinuous at zero velocity, it is not a straightforward problem to implement it in an active haptic device controlled with a discrete-time controller. For example, when the actuator force from the haptic device is determined so that it opposes the measured velocity, the repetition of zero-velocity crossing results in high-frequency oscillation in the actuator force, which is called chattering. A conventional remedy for this problem is to use a threshold below which the velocity is considered zero (i.e., to use a dead band on velocity) [7], but the system behavior is strongly influenced by the threshold. To avoid these problems, we have recently proposed discrete-time friction models based on implicit Euler method [8]. These models are originally restricted to homogeneous frictional systems.

The contributions of this paper can be broadly divided into two parts. The first one is an analytical model of the needle resistance force as a Coulomb-like friction force that depends on the penetration depth and the moving direction. In this model, a pop is resulted from a change in the contact angle at the contact point between the needle and the membrane. The second one is a discrete-time implementation of this model. We derive an extension of our previous friction models [8] to include the needle friction, which depends on the penetration depth and the moving direction of the needle. The presented model primarily targets shallow needle insertions, such as intravenous injection. Thus, this paper does not consider needle bending and tissue deformations in deep needle insertions, which were treated in [9, 10].

In what follows, section 2 formulates the needle resistance force as a depth-dependent, direction-dependent Coulomb-like friction force. Section 3 discusses a discrete-time implementation of the needle insertion friction. Section 4 presents an implementation demonstration using a PHANTOM Omni haptic interface. Section 5 provides the concluding remarks.

2 Needle Insertion/Withdrawal Force

2.1 Vertical Insertion/Withdrawal through Infinitely Thin Membrane

To extract fundamental mechanistic interactions that occur during a needle insertion, we start our analysis with a simple two-dimensional model. Consider the situation illustrated in Fig. 1, in which a wedge-shaped object is vertically thrusting into the gap between two point elements that are connected to each other via a spring. The wedge represents a needle and the pair of point elements represents an infinitely thin membrane to be punctured. The spring represents the resistance of the membrane against tangential extensions. Let κ be the spring coefficient of the spring and μ be the friction coefficient between the point elements and the needle. Let w be the needle's diameter (the width of the wedge in the 2-D model), and θ be the tip angle of the needle. We assume that there is a precompression force c in the spring.

Let q be the depth of the needle insertion, measured positive downward in Fig. 1. Then, the spring force, g, acting on the needle is determined as a function of q as follows:

$$g(q) = \begin{cases} 0 & \text{if } q < 0 \\ q\kappa \tan\theta + c & \text{if } q \in [0, w/\tan\theta] \\ \kappa w + c & \text{if } q > w/\tan\theta \end{cases} \quad (1)$$

There may be forces acting tangentially to the needle, but

*e-mail: kikuuwe@ieee.org

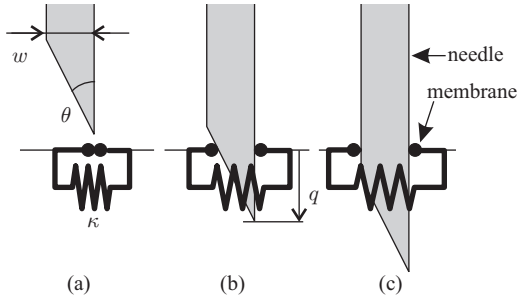

Figure 1: Wedge-like representation of a needle and an infinitely thin membrane.

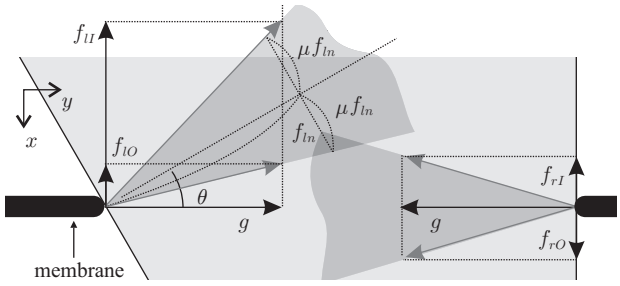

Figure 2: Friction cones on the needle tip.

we assume that tangential forces are small enough to be ignored.

Let us consider the situation of Fig. 1(b), in which the membrane is in contact with the needle tip. In this situation, the friction cones, which are the sets of possible forces acting on the needle, can be illustrated as Fig. 2. The vertex angle of both friction cones is $2\tan^{-1}\mu$. The sum of the forces from the both sides of the wedge is in the vertical direction (x direction in Fig. 2) because the forces balance each other in the horizontal direction (y direction in Fig. 2).

From (1), we know that the magnitude of the horizontal forces from the both sides of the wedge is $g(q)$. Therefore, a vertical force f_r acting on the right side (vertical face) of the wedge satisfies the following condition:

$$f_r \in [f_{rI}, f_{rO}], \quad f_{rI} = -\mu g(q), \quad f_{rO} = \mu g(q). \tag{2}$$

In other words, $[f_{rI}, f_{rO}]$ is the set of possible forces that can be produced when the needle is in static friction. The forces f_{rI} and f_{rO} represent the kinetic friction forces on the right side during insertion (going down) and withdrawal (going up), respectively.

The force from the left side (slanted face) is a little complicated. Let f_{ln} (> 0) be the magnitude of the normal force from the left side. Then, the lateral force $g(q)$ and the vertical force f_l satisfies

$$\begin{bmatrix} f_l \\ g(q) \end{bmatrix} = f_{ln} \begin{bmatrix} -\sin\theta \\ \cos\theta \end{bmatrix} + \alpha\mu f_{ln} \begin{bmatrix} -\cos\theta \\ -\sin\theta \end{bmatrix}, \tag{3}$$

where $\alpha \in [-1, 1]$. When α is between -1 and 1, the needle is in static friction. From (3), the normal force can be described as

$$f_{ln} = g(q)/(\cos\theta - \alpha\mu\sin\theta). \tag{4}$$

Substituting (4) into the first row of (3) yields

$$f_l = -g(q)\frac{\sin\theta + \alpha\mu\cos\theta}{\cos\theta - \alpha\mu\sin\theta} = -g(q)\frac{\tan\theta + \alpha\mu}{1 - \alpha\mu\tan\theta}. \tag{5}$$

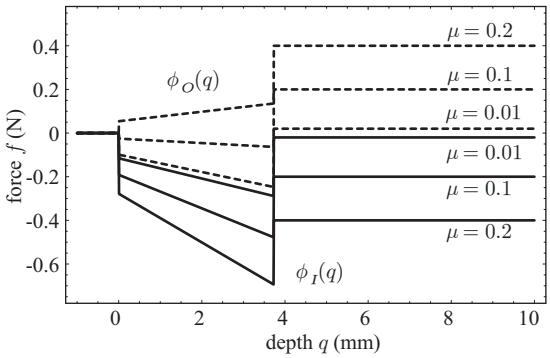

Figure 3: Numerical examples of $\phi_I(q)$ and $\phi_O(q)$: $w = 1$ mm, $\kappa = 0.6$ N/mm, $c = 0.4$ N, $\theta = \pi/12$ rad, $\mu = 0.01$, 0.1, and 0.2.

Because $\alpha \in [-1, 1]$, f_l satisfies the following condition:

$$f_l \in \begin{cases} [f_{lI}, f_{lO}] & \text{if } \mu\tan\theta < 1 \\ (-\infty, f_{lO}] & \text{if } \mu\tan\theta \geq 1 \end{cases}$$

$$f_{lI} = -g(q)\frac{\mu + \tan\theta}{1 - \mu\tan\theta}, \quad f_{lO} = g(q)\frac{\mu - \tan\theta}{1 + \mu\tan\theta}. \tag{6}$$

This means that

$$\mu\tan\theta < 1 \tag{7}$$

is the necessary condition for realizing needle insertion because otherwise an infinitely large negative (upward) force is possible. If (7) is satisfied, the forces f_{lI} and f_{lO} represent the kinetic friction forces experienced during insertion (going down) and withdrawal (going up), respectively.

Combining the forces from the both sides, we can see that the total resistance force acting on the needle satisfies the following condition:

$$f \in [f_I, f_O] \tag{8}$$

$$f_I = f_{rI} + f_{lI} = -(q\kappa\tan\theta + c)\frac{2\mu + (1-\mu^2)\tan\theta}{1 - \mu\tan\theta} \tag{9}$$

$$f_O = f_{rO} + f_{lO} = (q\kappa\tan\theta + c)\frac{2\mu - (1-\mu^2)\tan\theta}{1 + \mu\tan\theta}. \tag{10}$$

In the situation of Fig. 1(c), where the membrane is fully punctured and is in contact with the parallel portion (shaft) of the needle, the force acting on the needle is written as

$$f \in [f_I, f_O], \ f_I = -2\mu(\kappa w + c), \ f_O = 2\mu(\kappa w + c). \tag{11}$$

In conclusion, the resistance force experienced during needle insertion and withdrawal can be described as follows:

$$f \in [\phi_I(q), \phi_O(q)] \tag{12}$$

$$\phi_I(q) = \begin{cases} 0 & \text{if } q < 0 \\ -A_I(q+Q) & \text{if } q \in [0, X] \\ -F & \text{if } q > X \end{cases} \tag{13}$$

$$\phi_O(q) = \begin{cases} 0 & \text{if } q < 0 \\ A_O(q+Q) & \text{if } q \in [0, X] \\ F & \text{if } q > X, \end{cases} \tag{14}$$

where

$$\begin{aligned} X &= w/\tan\theta \\ A_I &= \kappa\tan\theta\left(2\mu + (1-\mu^2)\tan\theta\right)/(1 - \mu\tan\theta) \\ A_O &= \kappa\tan\theta\left(2\mu - (1-\mu^2)\tan\theta\right)/(1 + \mu\tan\theta) \\ Q &= c/(\kappa\tan\theta) \\ F &= 2\mu(\kappa w + c). \end{aligned} \tag{15}$$

Equation (15) implies that the set of parameters $\{X, A_I, A_O, Q, F\}$ satisfies $A_I > 0$, $A_O < A_I$, $A_I(X+Q) > F$, and $A_O(X+Q) < F$. Fig. 3 shows numerical examples of $\phi_I(\cdot)$ and $\phi_O(\cdot)$. The functions $\phi_I(q)$ and $\phi_O(q)$ are always discontinuous at $q = X$. The discontinuity in $\phi_I(\cdot)$ is felt as a pop during insertion.

2.2 Membrane with a Non-zero Thickness

Next, we derive a model in which the membrane has a non-zero thickness and the needle is inserted in a non-vertical direction. Let us consider a membrane with a thickness H and let β be the angle between the membrane's normal direction and the needle direction, as illustrated in Fig. 4. Assume that the magnitude of kinetic friction force is F when the needle tip vertically penetrated the membrane. We assume that this membrane can be regarded as a stack of infinitely thin membranes and the interaction among the membranes can be ignored. In this case, the membrane may apply a moment onto the needle around the contact point, but we ignore this effect. We concentrate on the resistance force in the axial direction of the needle.

The force from a membrane with an infinitesimal thickness dq is determined as $\phi_I(q)dq/H$ and $\phi_O(q)dq/H$ when it is punctured vertically. Then, the resistance force from the whole membrane with a thickness H is described as

$$f \in [\Phi_I(q), \Phi_O(q)]$$
$$\Phi_I(q) = \int_{q-U}^{q} \frac{\phi_I(\xi)}{H} d\xi, \quad \Phi_O(q) = \int_{q-U}^{q} \frac{\phi_O(\xi)}{H} d\xi, \quad (16)$$

where

$$U = H/\cos\beta. \quad (17)$$

This indicates that the needle resistance force depends on seven parameters, $\{X, A_I, A_O, Q, F, H, U\}$. Six of them, $\{X, A_I, A_O, Q, F, H\}$, depends on the properties of the needle, $\{w, \theta\}$, and those of the membrane, $\{c, \kappa, \mu, H\}$. The rest one, U, depends on the angle of insertion, β. Analytical expressions of $\Phi_I(q)$ and $\Phi_O(q)$ can be easily obtained by using (13) and (14) as follows:

$$\Phi_I(q) = \begin{cases} 0 & \text{if } q < 0 \\ -A_I q(q+2Q)/(2H) & \text{if } q \in [0, \min(U, X)] \\ -A_I U(2q - U + 2Q)/(2H) & \text{if } q \in [U, X] \\ -F(q-X)/H - A_I X(X+2Q)/(2H) & \text{if } x \in [X, U] \\ -F(q-X)/H - A_I(U+X-q)(q-U+X+ & \\ \quad 2Q)/(2H) & \text{if } q \in [\max(U, X), X+U] \\ -FU/H & \text{if } q > X+U \end{cases} \quad (18)$$

$$\Phi_O(q) = \begin{cases} 0 & \text{if } q < 0 \\ A_O q(q+2Q)/(2H) & \text{if } q \in [0, \min(U, X)] \\ A_O U(2q - U + 2Q)/(2H) & \text{if } q \in [U, X] \\ F(q-X)/H + A_O X(X+2Q)/(2L) & \text{if } q \in [X, U] \\ F(q-X)/H + A_O(U+X-q)(q-U+X+ & \\ \quad 2Q)/(2H) & \text{if } q \in [\max(U, X), X+U] \\ FU/H & \text{if } q > X+U. \end{cases} \quad (19)$$

Fig. 5 shows numerical examples of the functions $\Phi_I(q)$ and $\Phi_O(q)$ with varying thickness. The influence of pop becomes smaller as the thickness increases.

In conclusion, we have formulated the needle resistance force as a Coulomb-like friction force whose magnitude depends on the insertion depth and on the direction of the movement. The friction force f is written as follows:

$$f \begin{cases} = \Phi_I(q) & \text{if } \dot{q} > 0 \\ \in [\Phi_I(q), \Phi_O(q)] & \text{if } \dot{q} = 0 \\ = \Phi_O(q) & \text{if } \dot{q} < 0. \end{cases} \quad (20)$$

From (18) and (19), we have $\Phi_I(q) < \Phi_O(q)$, $\Phi_I(q) \geq 0$, and $\Phi_I(q) = \Phi_O(q) = 0$ $\forall q < 0$.

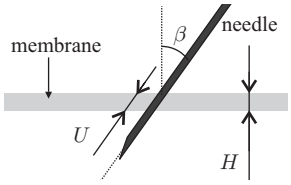

Figure 4: Needle Insertion through a membrane with a non-zero thickness.

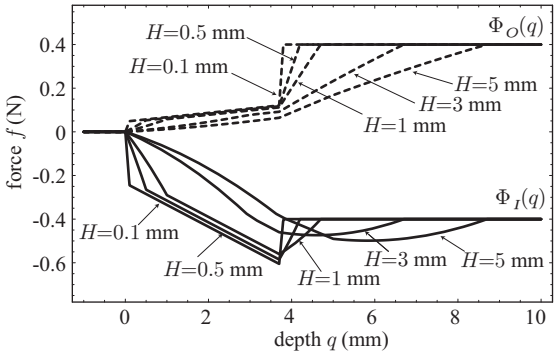

Figure 5: Needle resistance force during vertical penetrations: $w = 1.08$ mm, $\kappa = 0.57$ N/mm, $c = 0.41$ N, $\theta = 0.28$ rad, $\mu = 0.2$, $\beta = 0$, and $H = 5, 3, 1, 0.5, 0.1$ mm.

3 Discrete-Time Implementation

3.1 One-Dimensional Model

We consider to implement the Coulomb-like friction characteristics of (20) in discrete time. Because the definition (20) is indeterminate at $\dot{q} = 0$ and is discontinuous with respect to $\dot{q}$ at $\dot{q} = 0$, it is not a straightforward problem to implement (20) in discrete-time systems. We previously proposed discrete-time friction models [8] that employ the implicit Euler method to treat the indeterminacy and the discontinuity at the zero velocity. We here present an extension of their model to include the dependence on the position (q, in this case) and direction.

We start our discussion from a one-dimensional model of needle friction. Let T be the sampling interval and $p(k)$ be the position (in the direction of the needle movement) of the haptic device measured by the position sensors at time instant kT, where k is an integer indicating a discrete-time index. We consider a virtual point-like, massless element, termed as a proxy, as illustrated in Fig. 6. Let $q(k)$ be the position of the proxy. The proxy is connected to the haptic device via a virtual spring-damper element, which is often termed as a virtual coupling. Then, the force $f(k)$ produced by the virtual coupling satisfies

$$f(k) = Ke(k) + B(e(k) - e(k-1))/T, \quad (21)$$

where

$$e(k) = q(k) - p(k). \quad (22)$$

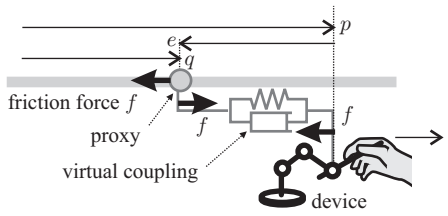

Figure 6: Proxy-based implementation of Coulomb friction.

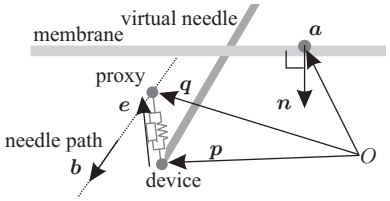

Figure 7: Three-dimensional model.

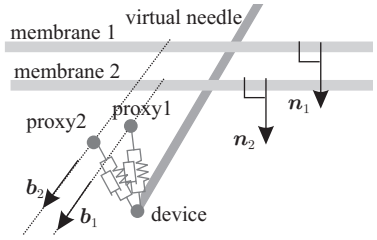

Figure 8: Multiple proxies for multiple-membrane puncture.

Here, K and B denote the spring and damper coefficients of the virtual coupling, respectively.

A friction force also acts on the proxy, as illustrated in Fig. 6. Because the proxy is massless, the friction force always balances the force from the virtual coupling. Therefore, the friction force is also denoted by $f(k)$. Based on (20), the friction force acting on the proxy satisfies

$$f(k) \begin{cases} = \Phi_I(q(k)) & \text{if } q(k)-q(k-1) > 0 \\ \in [\Phi_I(q(k)), \Phi_O(q(k))] & \text{if } q(k)-q(k-1) = 0 \\ = \Phi_O(q(k)) & \text{if } q(k)-q(k-1) < 0. \end{cases} \quad (23)$$

The force $f(k)$ should be chosen so that it satisfies both of (21) and (23). The force $f(k)$ is commanded to the actuator of the haptic device.

Equations (21), (22), and (23) represent algebraic constraints that must be satisfied in this system. Once the position $p(k)$ is provided, the output force $f(k)$ must be determined so as to satisfy these equations. Either of $e(k)$ or $q(k)$ has to be treated as a state variable.

Equation (23) can be rewritten as follows:

$$\begin{aligned} &(f(k) = \Phi_I(q(k)) \wedge q(k) - q(k-1) > 0) \\ &\vee (f(k) \in [\Phi_I(q(k)), \Phi_O(q(k))] \wedge q(k) - q(k-1) = 0) \\ &\vee (f(k) = \Phi_O(q(k)) \wedge q(k) - q(k-1) < 0)\,. \end{aligned} \quad (24)$$

Here, $\wedge$ and $\vee$ denote AND and OR operators, respectively. The unknown variables $q(k)$ and $e(k)$ can be eliminated by substituting (21) and (22) into (24). From (21), we have

$$e(k) = Be(k-1)/(KT+B) + Tf(k)/(KT+B). \quad (25)$$

By using the above and (22), we obtain

$$\begin{aligned} q(k) - q(k-1) &= p(k) + e(k) - p(k-1) - e(k-1) \\ &= T\left(f(k) - f^*(k)\right)/(KT+B), \end{aligned} \quad (26)$$

where

$$f^*(k) = -(KT+B)(p(k)-p(k-1))/T + Ke(k-1). \quad (27)$$

Substituting (26) into (24) yields

$$\begin{aligned} &(f(k) = \Phi_I(q(k)) \wedge f(k) > f^*(k)) \\ &\vee (f(k) \in [\Phi_I(q(k)), \Phi_O(q(k))] \wedge f(k) = f^*(k)) \\ &\vee (f(k) = \Phi_O(q(k)) \wedge f(k) < f^*(k))\,, \end{aligned} \quad (28)$$

which is equivalent to

$$f(k) = \begin{cases} \Phi_I\left(q(k)\right) & \text{if } f^*(k) < \Phi_I\left(q(k)\right) \\ f^*(k) & \text{if } f^*(k) \in [\Phi_I\left(q(k)\right), \Phi_O\left(q(k)\right)] \\ \Phi_O\left(q(k)\right) & \text{if } f^*(k) > \Phi_O\left(q(k)\right). \end{cases} \quad (29)$$

Equation (29) is still not a closed form because it contains $q(k)$, which depends on $f(k)$, in its right-hand side. Because of

$$q(k) = p(k) + (Be(k-1) + Tf(k))/(KT+B), \quad (30)$$

we can use

$$q^*(k) = p(k) + (Be(k-1) + Tf(k-1))/(KT+B) \quad (31)$$

as an approximation of $q(k)$. By using this, we can determine $f(k)$ as follows:

$$f(k) = \begin{cases} \Phi_I\left(q^*(k)\right) & \text{if } f^*(k) < \Phi_I\left(q^*(k)\right) \\ f^*(k) & \text{if } f^*(k) \in [\Phi_I\left(q^*(k)\right), \Phi_O\left(q^*(k)\right)] \\ \Phi_O\left(q^*(k)\right) & \text{if } f^*(k) > \Phi_O\left(q^*(k)\right). \end{cases} \quad (32)$$

Once $f(k)$ is obtained, the other unknown $e(k)$ can be determined by using (25).

In conclusion, the force $f(k)$ can be determined in the following procedure:

$$\boxed{\begin{aligned} q^*(k) &:= p(k) + (Be(k-1) + Tf(k-1))/(KT+B) \\ f^*(k) &:= -(KT+B)(p(k)-p(k-1))/T + Ke(k-1) \\ f(k) &:= \begin{cases} \Phi_I(q^*(k)) & \text{if } f^*(k) < \Phi_I(q^*(k)) \\ f^*(k) & \text{if } f^*(k) \in [\Phi_I(q^*(k)), \Phi_O(q^*(k))] \\ \Phi_O(q^*(k)) & \text{if } f^*(k) > \Phi_O(q^*(k)) \end{cases} \\ e(k) &:= (Tf(k) + Be(k-1))/(KT+B). \end{aligned}} \quad (33)$$

The computational procedure (33) provides an approximate solution for the algebraic equations (21), (22), and (23).

3.2 Three Dimensional Model

We can extend the one-dimensional model (33) into a three-dimensional model by considering forces and motions perpendicular to the needle's moving direction as illustrated in Fig. 7. We assume that the moving direction of the needle is determined when the needle enters the membrane, and this direction does not change until the needle is removed from the membrane. This assumption may appear unrealistic, but we use it because our primary target is relatively shallow needle insertions such as intravenous injection. This assumption will need to be removed to treat needle manipulations in a deep tissue.

Let $\boldsymbol{n}$ ($\|\boldsymbol{n}\| = 1$) be the inward normal direction of the membrane and $\boldsymbol{a}$ be an arbitrary point on the membrane surface. Let $\boldsymbol{b}$ ($\|\boldsymbol{b}\| = 1$) be the moving direction of the needle. Let $\boldsymbol{p}(k)$ be the actual position of the haptic device,

and $\boldsymbol{e}(k)$ be the displacement of the proxy with respect to the actual position. The proxy position is written as

$$\boldsymbol{q}(k) = \boldsymbol{p}(k) + \boldsymbol{e}(k). \tag{34}$$

The proxy is assumed to move only in the direction $\boldsymbol{b}$. This assumption is represented as

$$(\boldsymbol{I} - \boldsymbol{b}\boldsymbol{b}^T)(\boldsymbol{q}(k) - \boldsymbol{q}(k-1)) = \boldsymbol{o}, \tag{35}$$

where $\boldsymbol{o}$ is the three-dimensional zero vector and $\boldsymbol{I}$ is the three-dimensional identity matrix.

Due to the virtual coupling, the actuator force $\boldsymbol{f}(k)$ satisfies

$$\boldsymbol{f}(k) = K\boldsymbol{e}(k) + B(\boldsymbol{e}(k) - \boldsymbol{e}(k-1))/T. \tag{36}$$

From (34) and (36), we have

$$\boldsymbol{q}(k) - \boldsymbol{q}(k-1) = T(\boldsymbol{f}(k) - \boldsymbol{f}^*(k))/(KT + B), \tag{37}$$

where

$$\boldsymbol{f}^*(k) = -(KT + B)(\boldsymbol{p}(k) - \boldsymbol{p}(k-1))/T + K\boldsymbol{e}(k-1). \tag{38}$$

Because of (35) and (37), we obtain $(\boldsymbol{I} - \boldsymbol{b}\boldsymbol{b}^T)(\boldsymbol{f}(k) - \boldsymbol{f}^*(k)) = \boldsymbol{o}$, which is rewritten as

$$\boldsymbol{f}(k) = \boldsymbol{f}^*(k) + \boldsymbol{b}(\boldsymbol{b}^T\boldsymbol{f}(k) - \boldsymbol{b}^T\boldsymbol{f}^*(k)). \tag{39}$$

In this equation, $\boldsymbol{b}^T\boldsymbol{f}^*(k)$ and $\boldsymbol{b}^T\boldsymbol{f}(k)$ are correspondent to $f^*(k)$ and $f(k)$ in (33), respectively. Therefore, we can extend (33) into a three-dimensional model as follows:

$$\boxed{\begin{array}{l}
\boldsymbol{q}^*(k) := \boldsymbol{p}(k) + (B\boldsymbol{e}(k-1) + T\boldsymbol{f}(k-1))/(KT + B) \\
\boldsymbol{f}^*(k) := -(KT + B)(\boldsymbol{p}(k) - \boldsymbol{p}(k-1))/T + K\boldsymbol{e}(k-1) \\
q^*(k) := \boldsymbol{n}^T(\boldsymbol{q}^*(k) - \boldsymbol{a})/(\boldsymbol{n}^T\boldsymbol{b}) \\
f^*(k) := \boldsymbol{b}^T\boldsymbol{f}^*(k) \\
f(k) := \begin{cases} \Phi_I(q^*(k)) & \text{if } f^*(k) < \Phi_I(q^*(k)) \\ f^*(k) & \text{if } f^*(k) \in [\Phi_I(q^*(k)), \Phi_O(q^*(k))] \\ \Phi_O(q^*(k)) & \text{if } f^*(k) > \Phi_O(q^*(k)) \end{cases} \\
\boldsymbol{f}(k) := \boldsymbol{f}^*(k) + \boldsymbol{b}(f(k) - f^*(k)) \\
\boldsymbol{e}(k) := (B\boldsymbol{e}(k-1) + T\boldsymbol{f}(k))/(KT + B).
\end{array}} \tag{40}$$

Notice that $\boldsymbol{n}^T\boldsymbol{b} = \cos\beta$. The direction $\boldsymbol{b}$ can be determined when the needle enters the membrane. We can use $\boldsymbol{n}^T(\boldsymbol{q}^*(k) - \boldsymbol{a}) < 0$ as the condition to judge whether the needle is inside the membrane. The complete computational procedure that includes this judgment can be written as follows:

$$\boxed{\begin{array}{l}
\boldsymbol{q}^*(k) := \boldsymbol{p}(k) + (B\boldsymbol{e}(k-1) + T\boldsymbol{f}(k-1))/(KT + B) \\
\text{IF } \boldsymbol{n}^T(\boldsymbol{q}^*(k) - \boldsymbol{a}) \geq 0 \text{ THEN} \\
\quad \boldsymbol{f}(k) := 0 \\
\text{ELSE} \\
\quad \text{IF } \boldsymbol{n}^T(\boldsymbol{q}^*(k-1) - \boldsymbol{a}) \geq 0 \text{ THEN} \\
\quad\quad \boldsymbol{b} := \text{measured orientation of device} \\
\quad\quad U := L/(\boldsymbol{n}^T\boldsymbol{b}) \quad \text{/* used in } \Phi_I(\cdot) \text{ and } \Phi_O(\cdot) \text{ */} \\
\quad \text{ENDIF} \\
\quad \boldsymbol{f}^*(k) := -(KT + B)(\boldsymbol{p}(k) - \boldsymbol{p}(k-1))/T + K\boldsymbol{e}(k-1) \\
\quad q^*(k) := \boldsymbol{n}^T(\boldsymbol{q}^*(k) - \boldsymbol{a})/(\boldsymbol{n}^T\boldsymbol{b}) \\
\quad f^*(k) := \boldsymbol{b}^T\boldsymbol{f}^*(k) \\
\quad f(k) := \begin{cases} \Phi_I(q^*(k)) & \text{if } f^*(k) < \Phi_I(q^*(k)) \\ f^*(k) & \text{if } f^*(k) \in [\Phi_I(q^*(k)), \Phi_O(q^*(k))] \\ \Phi_O(q^*(k)) & \text{if } f^*(k) > \Phi_O(q^*(k)) \end{cases} \\
\quad \boldsymbol{f}(k) := \boldsymbol{f}^*(k) + \boldsymbol{b}(f(k) - f^*(k)) \\
\text{ENDIF} \\
\boldsymbol{e}(k) := (B\boldsymbol{e}(k-1) + T\boldsymbol{f}(k))/(KT + B).
\end{array}} \tag{41}$$

If one needs to use a haptic device having no orientation sensors, $\boldsymbol{b}$ may be determined by the moving direction of the needle. In this case, the 6th line of (41) must be modified accordingly.

A simulation involving multiple membranes can be realized by using multiple proxies and multiple virtual couplings, as illustrated in Fig. 8; a pair of a proxy and a virtual coupling is necessary for one membrane. In this case, the force commanded to the actuator should be the sum of the forces from all virtual couplings.

4 Implementation Experiment

The proposed algorithm (41) was implemented in a SensAble PHANTOM Omni$^{\text{TM}}$ device[1]. This device is capable of three degree-of-freedom actuation and six degree-of-freedom measurements. The sampling interval was set to be $T = 1/1600 = 0.000625$ sec. The stylus of the PHANTOM device was manually operated by an experimenter.

Fig. 9 shows a typical screen shot of the graphical interface developed so that the experimenter can visually recognize a virtual needle and virtual membranes. The position of the rotational joint that connects the haptic interface to the stylus was matched with the position of the tip of the virtual needle. The normal vectors of the virtual membranes were set as $\boldsymbol{n} = [0, 1, 0]^T$. That is, the membranes were placed perpendicular to the y axis. The parameters for the virtual coupling were set as $K = 0.4$ N/mm and $B = 0.001$ Ns/mm. The parameters for the functions $\phi_I(\cdot)$ and $\phi_O(\cdot)$ were chosen as $\{w, \kappa, c, \theta, \mu\} = \{1.08$ mm, 0.57 N/mm, 0.41 N, 0.28 rad, 0.2 $\}$, which were the same as those used in the numerical examples of Fig. 5. The position data obtained from the encoders were smoothed with a first order low-pass filter with a cut-off frequency of 300 Hz.

In the experiment, the experimenter held the stylus of the haptic device and repeatedly inserted and withdrew the virtual needle into/from the virtual membrane in an approximately perpendicular direction. Three trials were performed on different targets: a thin membrane ($H = 0.1$ mm), a thick membrane ($H = 4.0$ mm), and a pair of membranes ($H = 1.0$ mm and 0.5 mm) separated by a distance of 3 mm. Fig 10, Fig 11, and Fig 12 show the results, representing plots of f_y versus p_y. The figures show that the proposed model produces qualitatively proper results including pop features. Because the proposed model is inherently based on Coulomb friction, a user can move the needle back and forth at arbitrary depth.

5 Conclusions

We have proposed an analytical model for resistance force experienced when a needle is inserted into and withdrawn from membranes. Besides, we have presented a discrete-time representation of this model to be implemented in haptic devices. The proposed model captures the 'pop' feature, which is a loss of resistance force experienced when the needle punctures a membrane. This model captures both insertion and withdrawal process, and captures static friction. The primary target for the proposed model is shallow needle insertions such as intravenous injections. The proposed model realizes computational efficiency by excluding needle bending and deformation of the membranes.

[1] http://www.sensable.com/products/phantom_ghost/phantom-omni.asp

In future studies, the proposed model must be verified by comparison with experimental data obtained from real needle insertion/withdrawal process. In particular, the influences of fracture and plastic deformation of membranes will need to be clarified. Moreover, the proposed model must be validated also through psychophysical studies for supporting subjective reality felt by human users. A haptic device with lower inertia and lower joint friction may be necessary for such experiments.

References

[1] M. Ursino, J. L. Tasto, B. H. Nguyen, R. Cunningham, and G. L. Merril, "CathSim^{TM}: an intravascular catheterization simulator on a PC," *Studies in Health Technology and Informatics*, vol. 62, pp. 360–366, 1999.

[2] T. Dang, T. M. Annaswamy, and M. A. Srinivasan, "Development and evaluation of an epidural injection simulator with force feedback for medical training," *Studies in Health Technology and Informatics*, vol. 81, pp. 97–102, 2001.

[3] P. N. Brett, T. J. Parker, A. J. Harrison, T. A. Thomas, and A. Carr, "Simulation of resistance forces acting on surgical needles," *Proc. of the Institution of Mechanical Engineers, Part H: J. of Engineering in Medicine*, vol. 211, pp. 335–347, 1997.

[4] H. Kataoka, T. Washio, K. Chinzei, K. Mizuhara, C. Simone, and A. M. Okamura, "Measurement of tip and friction force acting on a needle during penetration," in *Proc. of the 5th Int. Conf. on Medical Image Computing and Computer Assisted Intervention (MICCAI)*, 2002, pp. 216-223.

[5] A. M. Okamura, C. Simone, and M. D. O'Leary, "Force modeling for needle insertion into soft tissue," *IEEE Trans. on Biomedical Engineering*, vol. 10, no. 51, pp. 1707–1716, 2004.

[6] L. M. Batteau, A. Liu, J. B. A. Maintz, Y. Bhasin, and M. W. Bowyer, "A study on the perception of haptics in surgical simulation," in *Proc. of the Int. Symp. on Medical Simulation*, vol. 3078 of Lecture Notes in Computer Science, Springer-Verlag, 2004, pp. 185–192.

[7] D. Karnopp, "Computer simulation of stick-slip friction in mechanical dynamic systems," *Trans. of the ASME: J. of Dynamic Systems, Measurement, and Control*, vol. 107, no. 1, pp. 100–103, 1985.

[8] R. Kikuuwe, N. Takesue, A. Sano, H. Mochiyama, and H. Fujimoto, "Fixed-step friction simulation: From classical Coulomb model to modern continuous models," in *Proc. of the 2005 IEEE/RSJ Int. Conf. On Intelligent Robots and Systems*, 2005, pp. 3910–3917.

[9] S. P. DiMaio and S. E. Salcudean, "Interactive simulation of needle insertion models," *IEEE Trans. on Biomedical Engineering*, vol. 52, no. 7, pp. 1167–1179, 2005.

[10] R. J. R. Webster, N. J. Cowan, G. Chirikjian, and A. M. Okamura, "Nonholonomic modeling of needle steering," in *Proc. of the 9th Int. Symp. on Experimental Robotics*, 2004, pp. 35-44.

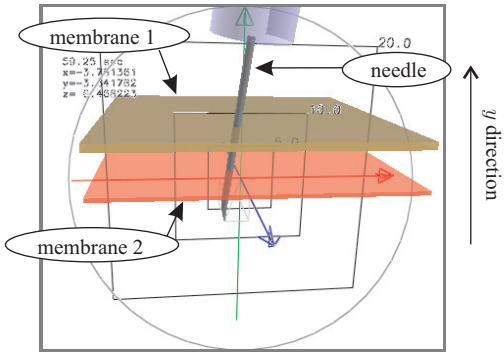

Figure 9: Screen shot of the simulator.

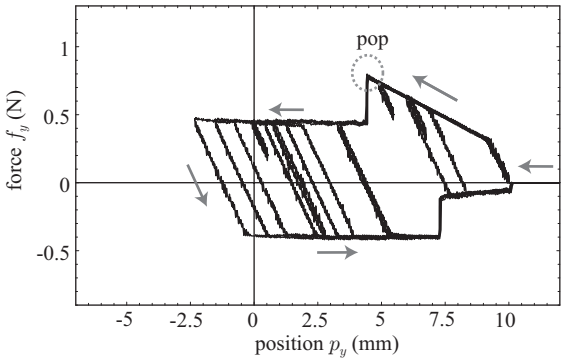

Figure 10: Actuator force during punctuating a thin membrane ($H = 0.1$ mm).

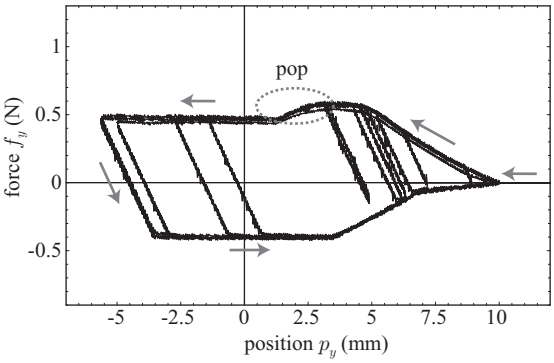

Figure 11: Actuator force during punctuating a thick membrane ($H = 4.0$ mm).

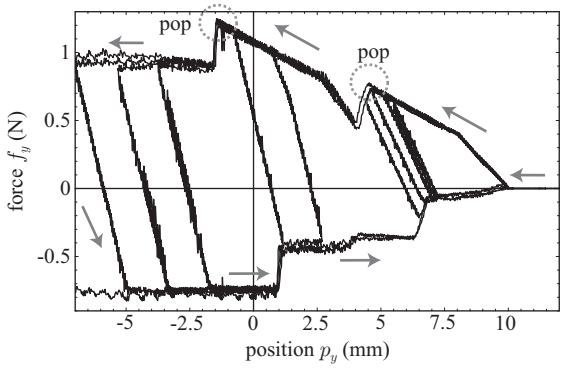

Figure 12: Actuator force during punctuating two membranes ($H = 1.0$ mm and 0.5 mm). This is the situation of Fig. 9.